Cattania, C., Rivalta, E., Hainzl, S., Passarelli, L., Aoki, Y. (2017): A non-planar slow rupture episode during the 2000 Miyakejima dike intrusion. - *Journal of Geophysical Research*, *122*, 3, pp. 2054—2068.

DOI: http://doi.org/10.1002/2016JB013722

AGU PUBLICATIONS

JGR

Journal of Geophysical Research: Solid Earth

RESEARCH ARTICLE
10.1002/2016JB013722

A nonplanar slow rupture episode during the 2000 Miyakejima dike intrusion

Camilla Cattania[1], Eleonora Rivalta[1], Sebastian Hainzl[1], Luigi Passarelli[1], and Yosuke Aoki[2]

[1]GFZ German Research Center for Geosciences, Potsdam, Germany, [2]Earthquake Research Institute, University of Tokyo, Tokyo, Japan

Key Points:
- During the 2000 Miyakejima dike intrusion we detect short bursts of seismicity lasting a few hours and propagating along the dike
- The surface deformation during the largest burst is best explained by aseismic slip taking place on the same faults as the earthquakes
- Intermittent slip episodes with a large aseismic component may accommodate a significant fraction of strain during diking

Supporting Information:
- Supporting Information S1

Correspondence to:
C. Cattania,
camcat@gfz-potsdam.de

Citation:
Cattania, C., E. Rivalta, S. Hainzl, L. Passarelli, and Y. Aoki (2017), A nonplanar slow rupture episode during the 2000 Miyakejima dike intrusion, *J. Geophys. Res. Solid Earth*, *122*, 2054–2068, doi:10.1002/2016JB013722.

Received 4 NOV 2016
Accepted 1 FEB 2017
Accepted article online 6 FEB 2017
Published online 4 MAR 2017

Abstract Magmatic intrusions release extensional strain in the Earth's crust upon availability of magma. Intrusions are typically accompanied by earthquake swarms and by surface faulting that is often larger than what is expected from the magnitude of the induced earthquakes. The 2000 Miyakejima dike intrusion triggered the largest volcanic earthquake swarm monitored so far, with five $M_l > 6$ earthquakes. We analyze the seismicity and deformation induced by the Miyakejima dike with the aim of constraining the timescale and mechanisms of slow strain release during the episode. In six earthquake bursts lasting few hours and migrating at ~1 km h^{-1} we find candidates for slow earthquakes. Each burst nucleated at the tips of previous bursts, suggesting stress interaction. The variability of fault plane solutions indicates that the bursts occurred on a complex system of fractures, consistent with weakly consolidated surface layers strained by spatially inhomogeneous stresses that change in time, such as those induced by a dike. Based on dislocation models, we find that deformation is best explained by aseismic slip (in addition to the seismic burst), with a moment 1.3 to 2.3 times larger than the earthquakes' seismic moment, and opening of 0.20 ± 0.07 m on the dike. The aseismic slip occurred over a few hours, with moment, duration, and migration velocity consistent with that of previously observed slow slip events. We argue that the seismic bursts are likely driven by slow slip, sharing most properties with tectonic slow slip events and swarms, but occurring on a set of nonaligned faults.

1. Introduction

Magmatic dikes are often associated with vigorous earthquake swarms, induced by the extensional stresses imparted by the dike at its propagating edge. For laterally propagating dikes, or dikes reaching close to the surface, the effect of the shallowest earthquakes is visible as graben faults. The many modern-day diking episodes monitored to date and frozen dikes studied in the field have revealed that dike-induced seismicity and faulting are complex processes.

Graben fault systems are characterized by a high degree of segmentation [*Mastin and Pollard*, 1988]. Long faults are thought to develop from linkages of smaller faults [*Segall and Pollard*, 1980], as also observed in analog experiments [*Xu et al.*, 2016]. Theoretical considerations of stresses imparted by dikes [*Rubin*, 1992], numerical models [*Buck et al.*, 2005], and observations [*Rowland et al.*, 2007] indicate that fault growth and linkage occur simultaneously to dike emplacement.

Focal mechanisms are often quite variable, although some dikes show a predominance of normal faulting [e.g., *Brandsdóttir and Einarsson*, 1979; *Shuler and Nettles*, 2012; *Belachew et al.*, 2013] and others of strike-slip mechanisms [e.g., *Ukawa and Tsukahara*, 1996; *Ágústsdóttir et al.*, 2016; *Ruch et al.*, 2016]. Considering the optimal orientation of faulting planes explains why strike-slip earthquakes are often observed ahead of or behind dikes and normal faulting above the dikes [*Rubin*, 1992; *Hill*, 1977; *Ágústsdóttir et al.*, 2016]. Oblique mechanisms may be similarly explained by the 3-D pattern of stresses around a penny-shaped or blade-like dike [*Passarelli et al.*, 2015a].

Slip on faults releases a variable fraction of the total moment released during diking, ranging from 0.01% to 50% [e.g., *Grandin et al.*, 2009; *Baer et al.*, 2008; *Nobile et al.*, 2012; *Pallister et al.*, 2010; *Wright et al.*, 2006; *Calais et al.*, 2008; *Pedersen et al.*, 2007] (see also supporting information Figure S1). Crustal deformation studies have

shown that a large fraction of this shear slip (20–90%) is aseismic [*Solomon et al.*, 1988] (supporting information Figure S1): the cumulative moment released seismically does not match the moment released on the graben faults, which may have lengths in excess of several tens of kilometers and throws of several meters. *Ruch et al.* [2016] found that the surface faulting during the 2014 Bárðarbunga-Holuhraun intrusion was not accompained by shallow seismicity but instead was entirely aseismic. Similarly, field studies of dike-induced swarms during the 2005 Dabbahu (Afar) dike intrusion [*Rowland et al.*, 2007] and the 1977 Krafla swarm [*Brandsdóttir and Einarsson*, 1979] indicate that fault activity occurred with a significant component of aseismic slip on faults with multiple orientations. Earthquakes with a large low-frequency component, indicative of slow rupture, have also been observed during other dike intrusions [*Pallister et al.*, 2010; *Belachew et al.*, 2011], including the Miyakejima intrusion [*Minson et al.*, 2007]. But while there is ample evidence for aseismic slip during graben faulting, the timescales and the precise mechanism involved in the aseismic strain release have not been constrained.

Recent decades have seen the discovery of several types of slow slip phenomena [*Ide et al.*, 2007; *Beroza and Ide*, 2011], which are now recognized as an important mode of stress release in subduction zones; they have also been reported in strike slip [*Linde et al.*, 1996; *Wei et al.*, 2013] including oceanic transform [*Lohman and McGuire*, 2007] faults. Slow slip phenomena are sometimes associated to seismic strain release, e.g., by tremor or migrating tectonic seismic swarms [*Peng and Gomberg*, 2010]. Several episodes of tectonic seismic swarms associated to aseismic slip events have been identified to date in all tectonic environments [e.g., *Yamaoka et al.*, 2005; *Borghi et al.*, 2016; *Kato et al.*, 2012; *Segall et al.*, 2006; *Passarelli et al.*, 2015b]. Also, in these cases, the observed ratio of aseismic to total moment released was very variable [e.g., *Villegas-Lanza et al.*, 2015; *Peng and Gomberg*, 2010]. The simultaneous seismic and aseismic release of strain is typically explained by the rupture of seismic patches surrounded by aseismic creep. In fact, the focal mechanisms in some cases of subduction zone slow slip events are uniform and consistent with the main fault plane [e.g., *Maury et al.*, 2016].

Whether dikes may cause slow slip events as they are understood in tectonic context is not known to date. Especially, there is a need to bridge the timescales of seismicity (a few seconds) to the timescales of structural geology/optical studies (a few days to weeks), in order to reveal if any of the swarm seismicity may be directly associated to additional aseismic slip. In this study, we use a combination of seismic and geodetic data to explore the dynamics of isolated seismicity bursts taking place during the 2000 Miyakejima dike intrusion. We constrain the timescale of this aseismic slip from the migration of the burst earthquake hypocenters. We also model the accompanying crustal deformation recorded by GPS stations by means of dislocation models constrained by the earthquakes' magnitudes and focal mechanism solutions. Finally, we discuss our findings based on previous results on slow earthquakes and argue that the Miyakejima bursts indicate progressive slow ruptures on a set of nonaligned faults.

2. The 2000 Miyakejima Seismic Swarm

The Miyakejima diking event started on 26 June 2000 at 18:00 (Japanese Standard Time, JST) on Miyake island. The seismicity then started to migrate away from the volcano, first radially to the west and then bending toward northwest toward Kozushima (Figure 1), covering a distance of ~30 km at a speed of $v \sim 4.4$ km/d. Then, the dike stopped due to the compression imparted by the topographic load of two more islands (Kozushima and Nijima) and slip on a preexisting strike-slip fault system it encountered on its way [*Maccaferri et al.*, 2015]. After arrest, the dike continued inflating and thickening and possibly growing vertically and backward, as revealed by geodetic models [*Ito and Yoshioka*, 2002; *Yamaoka et al.*, 2005; *Hughes*, 2010]. At the same time, several episodes of caldera collapse were recorded on Miyakejima [*Kumagai et al.*, 2001; *Geshi et al.*, 2012]. The seismic swarm lasted for about 3 months; the swarm is one of the largest ever recorded [*Toda et al.*, 2002], with five $M > 6$, almost 4900 $M_l \geq 3.0$ earthquakes, and a total seismic moment release equal to 3.6×10^{19} N m.

In this work we use the seismic catalog of the Japanese Meteorological Agency (JMA). A catalog has also been compiled by the Earthquake Research Institute of Japan (ERI), which included records from Ocean Bottom Seismometers (OBS) between 1 July and 2 August [*Sakai et al.*, 2001]. Comparison of the hypocenter depths in the two catalogs indicates that they are not well constrained: depths in the ERI catalog are more than 6 km shallower than in the JMA catalog (while differences in horizontal locations are less than 2 km). In addition, we use the focal mechanisms catalog from the Japan National Research Institute for Earth Science and Disaster Prevention (NIED).

The dike intrusion induced surface deformation which was recorded by the continuous GPS network installed by the Geospatial Information Authority of Japan (GEONET), which has stations on all of the four islands closest

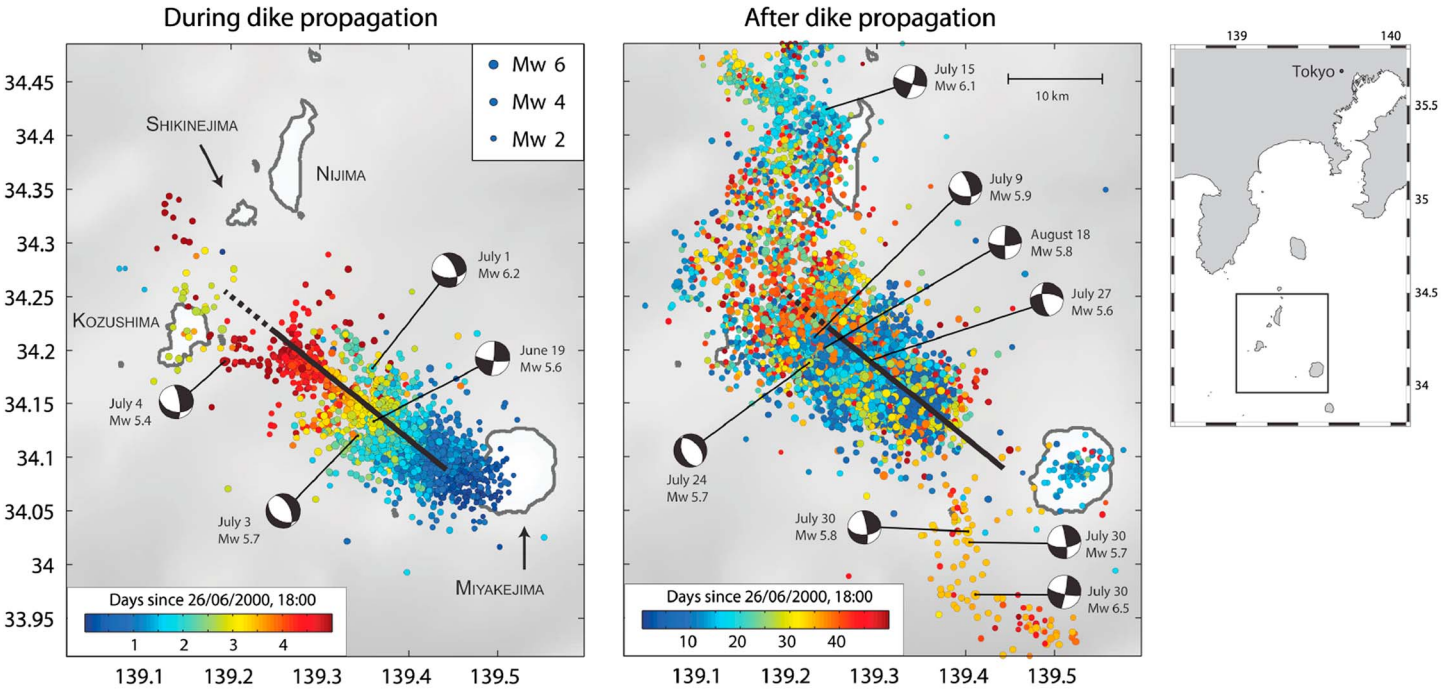

Figure 1. Map view of seismicity (left) during the dike propagation phase and (right) after the dike stopped, color coded by time. The black line indicates the inferred dike position, from *Hughes* [2010], and the dotted section indicates the segment which is not part of the dike according to the model of *Maccaferri et al.* [2015].

to the swarm (Miyakejima, Nijima, Kozushima, and Shikinejima). Daily solutions have been compiled by the Geospatial Information Authority of Japan.

During the dike stall and thickening phases, seismicity showed a complex pattern with the location of most intense activity moving back and forth along the dike (Figures 1 and 3). The events present a mixture of strike-slip and normal faulting mechanisms [*Passarelli et al.*, 2015a], and in some cases they have an opening component and a slow source process [*Minson et al.*, 2007]. In particular, we identified short bursts of seismicity lasting a few hours and lacking a causal main shock at the beginning of the sequence, which we now describe in detail.

3. Identification and Description of the Bursts

We considered bursts in the vicinity of the dike (within 5 km from the 30 km long dike trace shown in Figure 1) that occurred after the dike arrest (i.e., between 10 and 90 days since 26 June 2000). We identified all phases of unusually high seismicity rate by computing the β statistics [*Matthews and Reasenberg*, 1988; *Reasenberg and Simpson*, 1992], defined as

$$\beta(t, \Delta t) = \frac{n(t, \Delta t) - n_e(t, \Delta t)}{\sigma(t, \Delta t)} \tag{1}$$

where $n(t, \Delta t)$ is the number of events between t and $t + \Delta t$, $n_e(t, \Delta t)$ the expected number of events given a background rate, and $\sigma(t, \Delta t)$ its standard deviation. Most applications [e.g., *Matthews and Reasenberg*, 1988], assume a constant background rate λ, so that $n_e(t, \Delta t) = \sigma^2(t, \Delta t) = \lambda \Delta t$. However, in the present case we want to isolate seismicity bursts concurrent with the events triggered directly by dike growth. This process imposes a time-dependent stressing rate [e.g., *Hughes*, 2010], which is reflected in the background seismicity rate $\lambda(t)$ (Figure 2). To calculate the expected number of events in a time interval and the variance, we assume that background seismicity can be described as a nonstationary Poisson process [e.g., *Marsan*, 2003], so that the probability of n events in the interval $[t; t + \Delta t]$ is given by

$$P(N = n) = \frac{\Lambda^n(t, \Delta t)}{n!} e^{-\Lambda(t, \Delta t)} \tag{2}$$

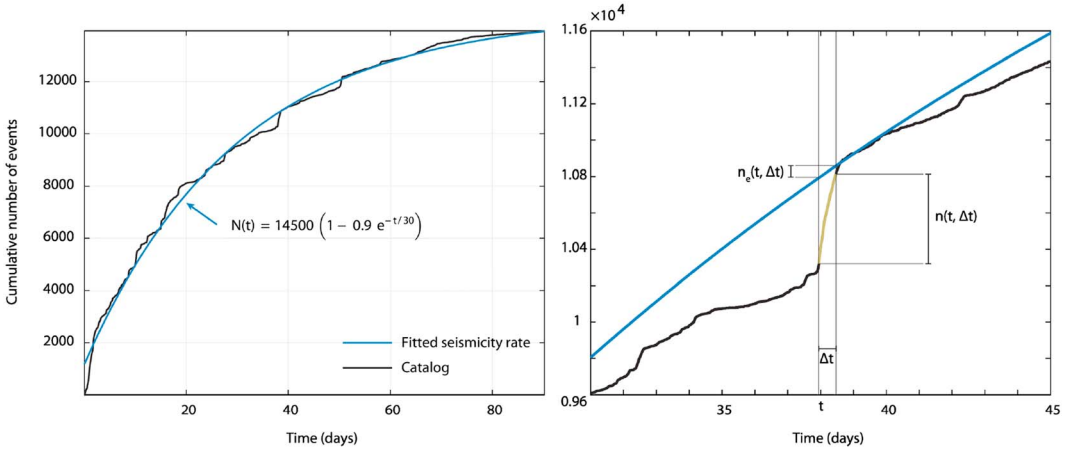

Figure 2. Example of burst detection by calculating the β value [*Matthews and Reasenberg*, 1988] with time-dependent background rate. (left) Cumulative number of events versus time from the catalog and fit with a decaying exponential function similar to the one suggested by *Rivalta* [2010]. (right) Example of a positive β anomaly (corresponding to largest burst detected, with $\beta = 58$).

with $\Lambda(t, \Delta t) = \int_t^{t+\Delta t} \lambda(t)\mathrm{d}t$. As for a stationary Poisson process, it can be shown that the expected number of events and the variance are given by $n_e(t, \Delta t) = \sigma^2(t, \Delta t) = \Lambda(t, \Delta t)$. Figure 2 shows the quantities involved in calculating β.

Since the duration of a burst is not known a priori, we followed the approach of *Matthews and Reasenberg* [1988] and calculated β for a range of Δt: we tested values between 2.4 h and 3 days, at 43 min intervals. For a given burst, the duration is identified by the maximum β value.

To isolate the most significant periods of enhanced seismicity, we define "burst" as a period in which $\beta \geq 20$, i.e., the seismicity rate is 20 standard deviations above the background rate. During the time period and distance specified above, we isolate six seismicity bursts with a duration between 3.1 and 13.2 h and between 141 and 529 events each (Table 1). Earthquakes within each bursts show migration of several kilometers either in the direction of dike propagation or backward, and in some cases bilateral propagation (Figure 3c).

The bursts partially overlap spatially, and the onset of each episode is close to the edge of the previous ones (Figures 3 and 4). We verified that this also occurs when choosing a lower threshold for detection ($\beta \geq 10$), as shown in Figure S2 of the supporting information. Individual bursts account for few percent of the total number of events and seismic moment in the 80 days considered (see Table 1), and cumulatively they constitute about 22% of the events and of the seismic moment released, even though they occur within only 2.4% of the time period.

Several main shocks ($M_w \geq 5.4$) occur during the time period considered, and their aftershock sequences may also result in β anomalies; in fact, we sometimes detect potential bursts with $t < t_{\mathrm{main}} < t + \Delta t$, in which case

Table 1. Summary of the Swarms Identified Between 10 and 90 Days Since 26 June 2000 and 5 km From the Dike[a]

Number	Date (JST)	Days Since 26 June 2000	Duration (h)	Percentage of Events	Percentage of Seismic Moment
1	06 Jul 2000 (18:00:00)	10.0	8.16	5.7	3.9
2	11 Jul 2000 (18:14:24)	15.0	3.12	2.7	1.1
3	15 Jul 2000 (03:36:00)	18.4	4.56	2.4	0.8
4	24 Jul 2000 (03:36:00)	27.4	3.12	1.6	2.9
5	03 Aug 2000 (16:19:12)	37.9	13.20	5.9	8.0
6	15 Aug 2000 (22:04:48)	50.2	10.32	4.0	4.2

[a]Percentages of number of events and seismic moment are with respect to all events in the same spatiotemporal window.

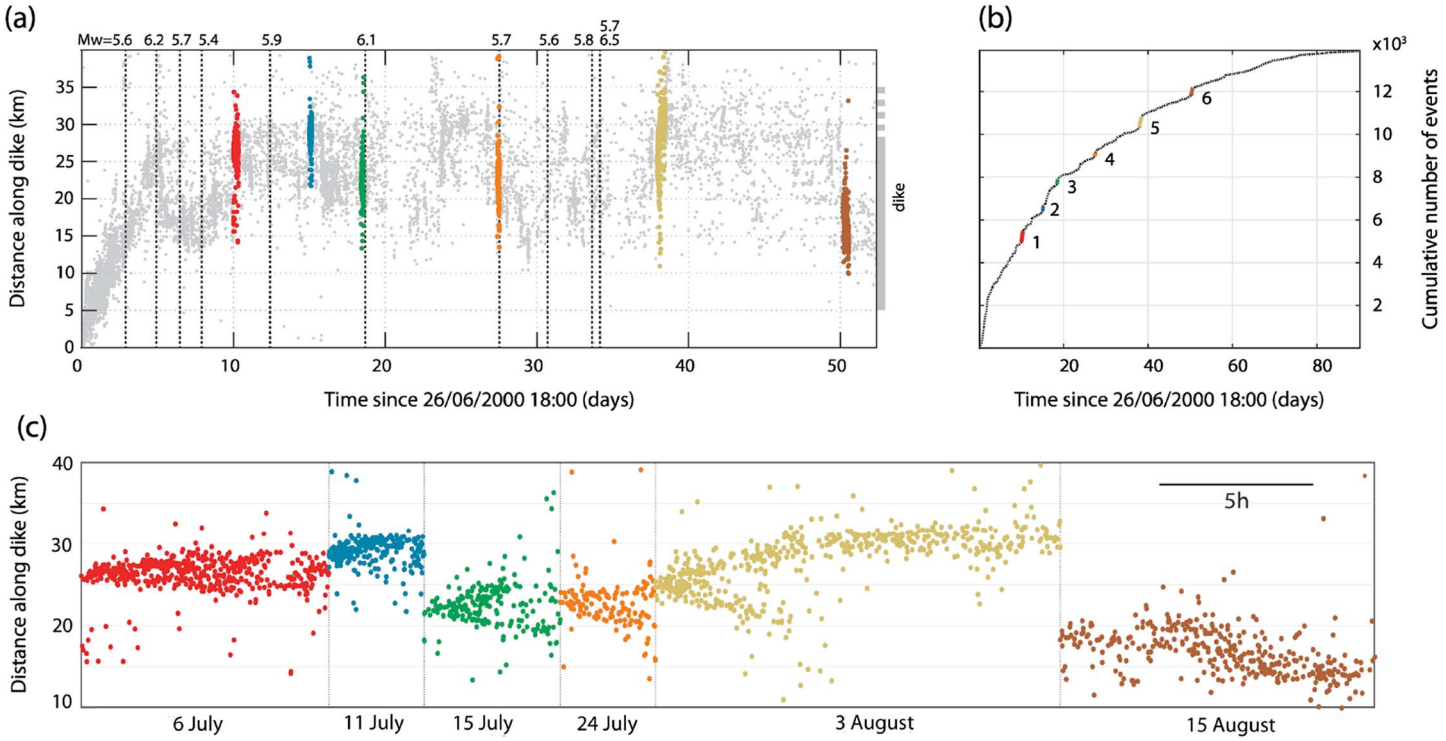

Figure 3. Summary of observed bursts in the phase following dike arrest. (a) Seismicity migration along the dike, from the catalog of the Japan Meteorological Agency (JMA). Colored events are identified as periods of elevated activity ("bursts"). The grey bar on the right indicates the dike extension according to *Hughes* [2010] (see Figure 1). (b) Cumulative number of events versus time, with bursts marked in different colors. (c) Migration of individual bursts, shown back to back to highlight their relative position and separated by the vertical lines.

the β anomaly may be due to aftershocks. In these cases we recalculated β for the interval $[t, t_{main}]$, so that only events prior to the main shock are accounted for.

We chose a rather high threshold for β, and all the bursts detected are also clearly visible by eye as steps in the cumulative number of events versus time plot (Figure 3b). We also verified that all these bursts correspond to periods of elevated seismicity rate according to the Z test [*Habermann*, 1983; *Wiemer*, 2001]

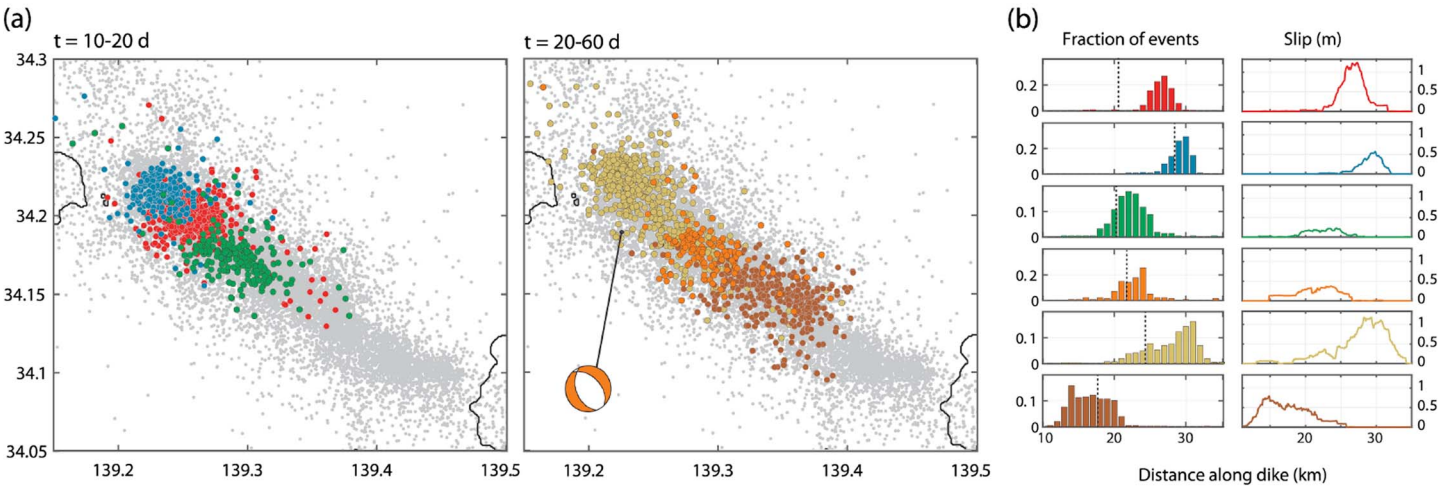

Figure 4. Spatial distribution of the bursts. (a) Map view, with bursts colored to match Figure 3. Grey dots are all events in the 90 days starting from 26 June 2000, 18:00 (JST). The fourth burst ends with a main shock M_w5.7, with the focal mechanism shown. (b) Distribution of events within each burst as a function of distance along the dike and estimated cumulative slip, calculated from empirical relations [*Wells and Coppersmith*, 1994]. Note the different scales in the y axis. The dotted lines indicate the location where the burst started, estimated from the mean epicenter of the first 10% of the events.

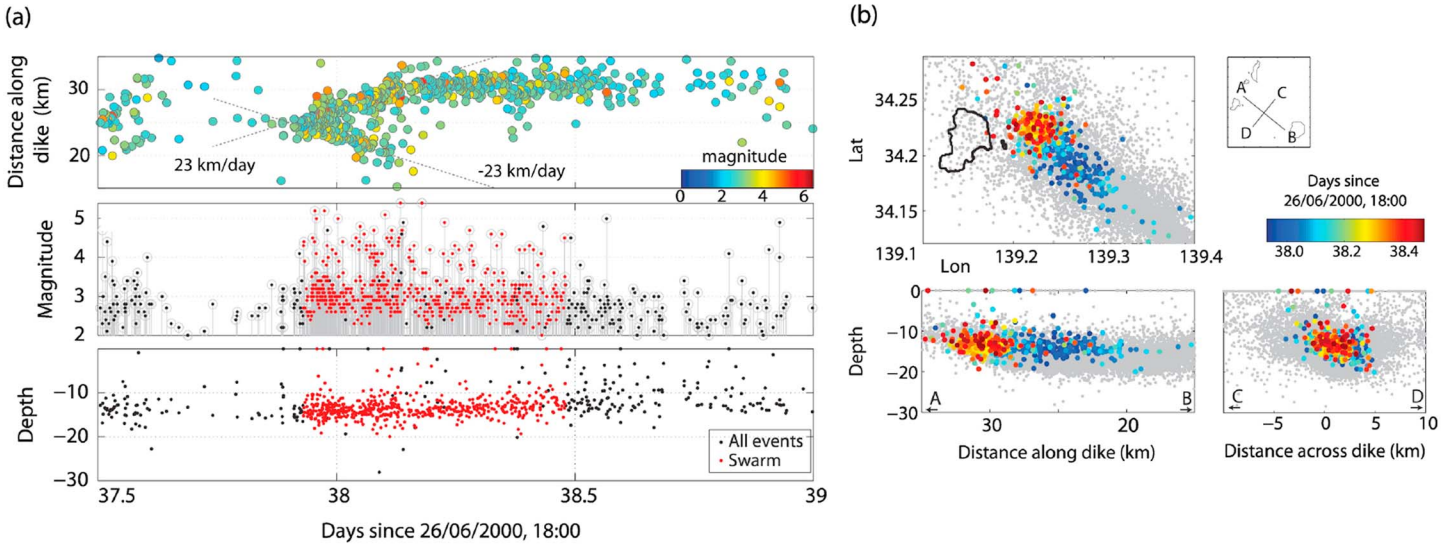

Figure 5. The 3 August burst, from the JMA catalog. (a) (top) Distance along the B-A segment (shown in the small map) versus time, showing the bidirectional propagation at a speed of ~23 km/d. (middle) Magnitude distribution with time. The events in red are within 5 km from the dike and in the time span indicated in Table 1, and they are those plotted in Figure 5b. (bottom) Depth versus time, showing a slight upward migration. (b) Map view and transects of the burst, color coded by time. Grey dots in Figure 5b are all earthquakes between 26 June 2000 and 1 January 2014.

(supporting information Figure S1). We note that both the β test and the Z test present several other instances of elevated seismicity rate which may potentially indicate additional bursts: the events presented here constitute a conservative estimation.

4. Analysis of the Largest Burst

The largest burst occurred on 3 August 2000 (Figure 5). The Japan Meteorological Agency catalog reports 529 $M_j \geq 1.9$ events, most of which had a magnitude between 2.0 and 3.5. The focal mechanisms catalog reports $M_w = 5.4$ for the largest event, while the burst cumulative seismic moment is equivalent to a $M_w 5.9$ earthquake. There was no large event at the start of the burst, indicating that this was not an aftershock sequence (Figure 5a). The most striking feature of this sequence is the bilateral migration at a speed of ~23 km/d (0.27 m/s) with a duration of ~5–7 h. Seismicity then stopped in the SE direction, while it continued in the NW direction. A slight upward migration is visible (Figure 5), even though vertical migration is difficult to establish due to uncertainties in the hypocenter depths. There is no evidence of migration in the direction perpendicular to the dike. While most seismicity appears confined along the length of the dike inferred by geodetic models, the NW edge of seismicity may be located above the dike or ahead of its tip, due to uncertainties in the dike models [*Hughes*, 2010; *Maccaferri et al.*, 2015] (Figure 6).

Focal mechanisms from the NIED catalog (available for a subset of the earthquakes) present a high degree of variability with normal, oblique, and strike-slip events (Figure 6). Using the focal mechanisms clustering algorithm developed by *Cesca et al.* [2014], we identify two predominant groups of events with different degree of normal and strike-slip components and different focal plane orientation. We do not find a clear dependence of focal mechanisms with time or epicenter location, while we note that all predominantly normal faulting events (cluster 1) are shallow, at 5 km depth. We find a similar distribution when considering the focal mechanisms from all the six bursts, which is also in agreement with the overall codiking seismicity [*Passarelli et al.*, 2015a]. This variability of focal mechanism indicates that the burst does not take place on a single smooth fault.

The 3 August burst is associated with deformation recorded by GPS. Daily GPS measurements show a baseline displacement of 6 ± 0.7 cm recorded by GPS stations on Niijima and Kozushima (sites 93057 and 93058 in Figure 7) between 3 August 2000, 12:00 and 4 August 2000, 12:00 (GMT), while other stations do not show a clear signal during this event. We note that in the previous day the baseline displacement was higher than normal (3 ± 0.7 cm, about 3 times higher than in the previous week), suggesting that an aseismic source was already active.

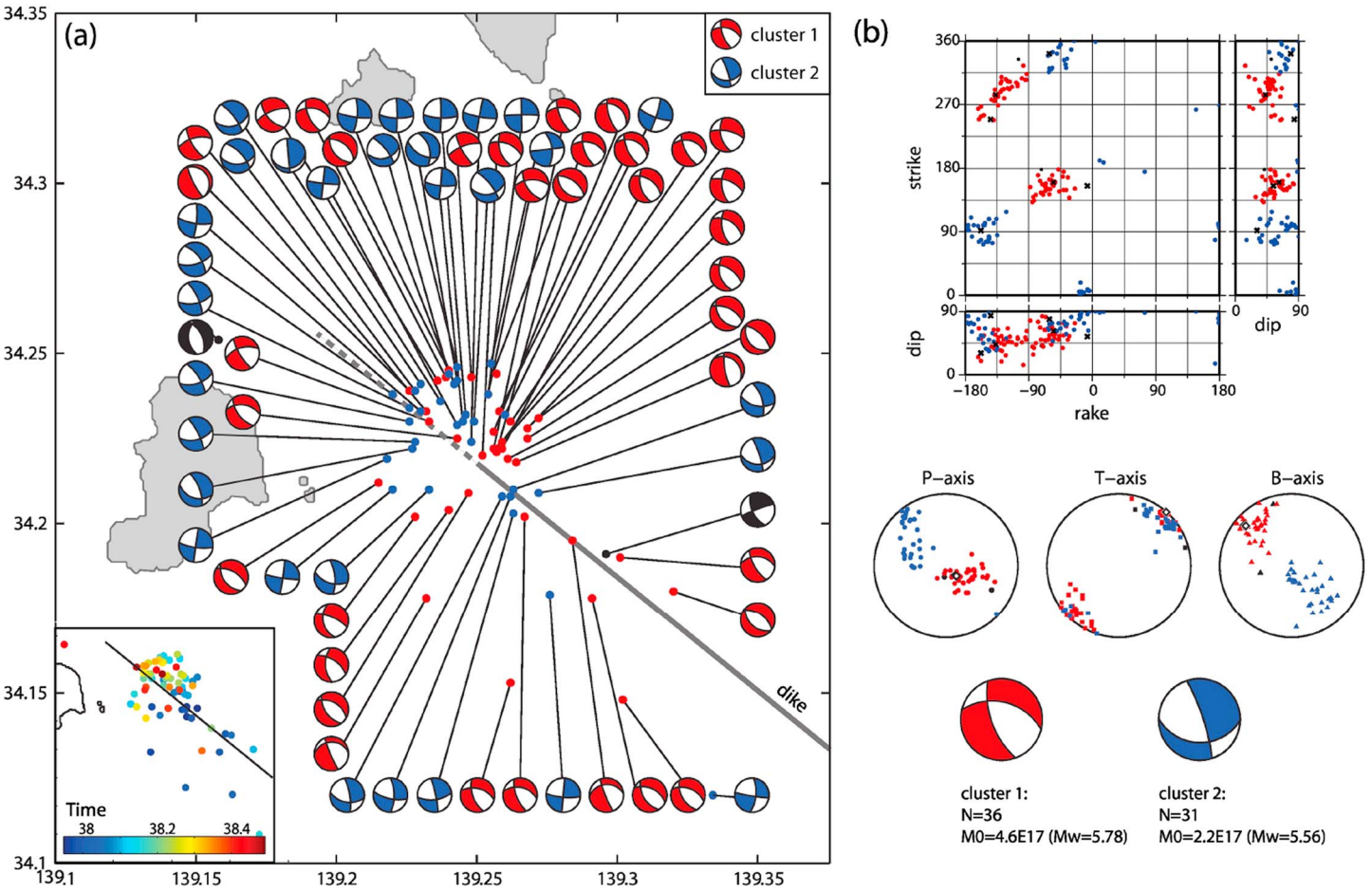

Figure 6. Focal mechanisms of the earthquakes in the 3 August burst. (a) Map view with events color coded by the cluster they belong to, calculated using the algorithm described by *Cesca et al.* [2014]. Black events are not in any cluster. (inset) Events are color coded by time. (b) Distribution of focal mechanisms parameters and focal axis. At the bottom, the mean focal mechanism for each cluster is shown, with their number of events and cumulative seismic moment.

5. Modeling Deformation Sources

We test different elastic dislocation models to explain the GPS recordings. Physically plausible deformation sources include the following: seismic slip only (Model 0), seismic slip plus opening on the dike representing the background dike growth (Model 1), seismic plus aseismic slip (Model 2), and seismic plus aseismic slip plus opening on the dike (Model 3). In what follows we describe how we compare and construct the models.

We compare the elastic deformation predicted in each case with 1 day of GPS data from Kozushima, Niijima, and Shikinejima. We do not include other stations because they may be affected by concurrent processes (in particular caldera collapse on Miyakejima). In all models, free parameters are estimated by minimizing least squares. We propagate uncertainties in the surface displacements (4 mm horizontal, 8 mm vertical) to estimate errors in the model parameters. Since we tested models with 0 to 2 degrees of freedom, we compare them by using a metric which not only takes into account model fit to the data but also penalizes models with more free parameters. This is the adjusted least squares R^2 value, given by

$$\bar{R}^2 = R^2 - \left(1 - R^2\right) \frac{p}{n - p - 1}$$

where n is the sample size (12), p the number of free parameters, and

$$R^2 = 1 - SS_{\text{res}}/SS_{\text{tot}}$$

with $SS_{\text{tot}} = \sum_i w_i \left(y_i - \bar{y}\right)^2$ and $SS_{\text{res}} = \sum_i w_i \left(y_i - f_i\right)^2$, where y_i are the observed displacements, $\bar{y}$ is their average, f_i are the modeled displacements, and w_i the weights (which are inversely proportional to the data error). The index i refers to stations and components.

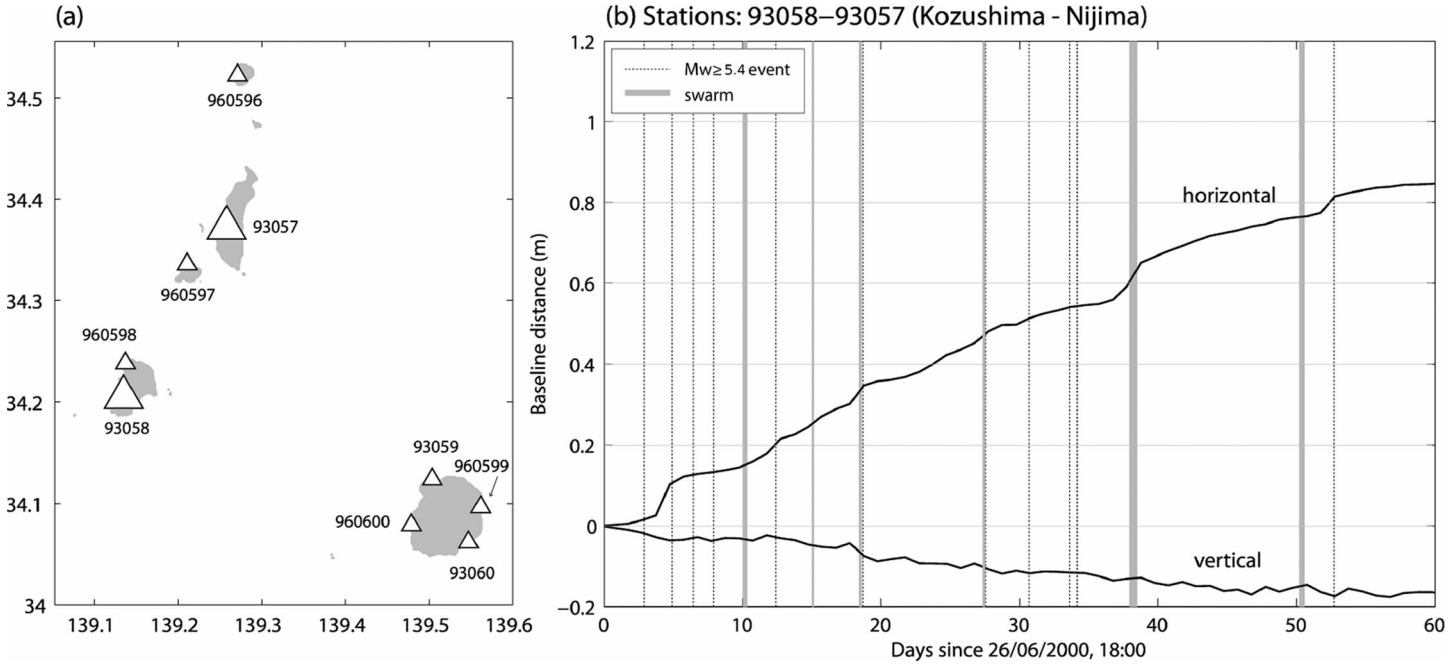

Figure 7. Observed crustal deformation. (a) Map of GEONET stations on the northern Izu islands. The two larger triangles are the stations used in Figure 7b. (b) Daily measurements of baseline distance in the first 60 days. The largest earthquakes and the time of the bursts are indicated by vertical lines.

5.1. Model 0—Seismicity Alone

To estimate seismic sources, we considered all earthquakes with a known focal mechanism and estimated the slip and fault dimension from the magnitude using the empirical relations of *Wells and Coppersmith* [1994] assuming a square fault. Even though focal mechanisms are only available for a subset of the events, we verified that they account for the vast majority of the seismic moment obtained from the more complete JMA catalog. Therefore, we do not expect the completeness of the focal mechanisms catalog to significantly affect the results.

We used all the events within the day and not only those which are part of the burst (five additional events). We tested alternative ways of choosing one of the two focal mechanisms for each event: (1) choosing all the planes dipping to the northeast of the dike, (2) choosing all the planes dipping to the southwest of the dike, (3) choosing the plane with the strike closest to the dike strike, (4) choosing the plane dipping toward the dike, and (5) choosing a random plane. We found only negligible difference in the modeled surface deformation (point source approximation). The results presented here are from choosing the plane with the strike closest to the dike. A further source of uncertainty in the focal planes solutions is the presence of non-double-couple components, which have been found to occur for several of the events in this data set [*Minson et al.*, 2007] and may bias the orientation of the focal planes.

5.2. Model 1—Seismicity Plus Tensile Source

In this model, surface deformation is due to the contribution of the earthquakes (modeled as described above) and uniform opening on a rectangular surface, representing inflation of the dike. We estimate the location and orientation of the tensile source by fitting a vertical plane to the earthquake epicenters and assuming a vertical extent of the dike of 10 km (between 5 and 15 km). We fix the strike to that of the dike (N129°E). We test two different lengths: the lateral extent of the burst (12 km) or the entire length of the dike (30 km), and we find that the two models give a similar fit to the data. The position of the 12 km dike is also based on the earthquake epicenters, resulting in a small offset (∼1 km) from the dike model shown in Figure 6. The offset is within the variability of published geodetic dike models [*Hughes*, 2010; *Yamaoka et al.*, 2005] and is likely not resolved by the GPS network.

5.3. Model 2—Seismicity + Aseismic Slip

This model tests the hypothesis that aseismic slip takes place during the seismic swarm. Unlike most swarms associated to slow slip, the burst on 3 August did not take place on a single, smooth fault (Figure 6). We assume

Table 2. Summary of Tested Source Models and Their Performance, Quantified by the Adjusted R^2 Value ($\bar{R}^2$)[a]

Model Number	No. of Free Parameters	M_0 From Aseismic Slip (N m)	M_0 From Opening (N m)	$\bar{R}^2$	Range of $\bar{R}^2$	Fraction of Times Model Outperforms Model 3
0	0	0	0	0.39	0.19–0.51	0
1	1	0	$1.4 \pm 0.3 \times 10^{18}$	0.80	0.43–0.96	0.03
2	1	$2.1 \pm 0.3 \times 10^{18}$	0	0.83	0.42–0.97	0.10
3	2	$1.3 \pm 0.4 \times 10^{18}$	$0.7 \pm 0.2 \times 10^{18}$	0.89	0.45–0.98	-
3 (B)	2	$0.8 \pm 0.3 \times 10^{18}$	$0.3^{+0.4}_{-0.3} \times 10^{18}$	0.85	0.44–0.98	0.33

[a]The uncertainties are obtained by drawing 10^5 realizations of perturbed surface displacement data (assuming independent Gaussian errors). The last column reports the fraction of iterations in which each model has $\bar{R}^2$ higher than Model 3. The $\bar{R}^2$ value in the fifth column is calculated for unperturbed data.

that some aseismic slip accompanied each earthquake and took place on the same fault planes. We use the same geometry as for Model 0 and calculated the additional amount of slip required to fit the data. To keep the number of free parameters low, we assume that all earthquakes have the same ratio of seismic/aseismic slip and that the seismic and aseismic slip on each fault have the same direction of slip vector. With these constraints, the aseismic slip on a fault i is simply given by

$$s_{i(\text{aseismic})} = k \cdot s_{i(\text{seismic})}$$

Therefore, this model has a single degree of freedom (parameter k).

Increasing slip without changing the fault size results in higher stress drops, which is unphysical, since slow slip and low-frequency events are characterized by smaller stress drops than typical earthquakes [*Ide et al.*, 2007; *Brodsky and Mori*, 2007]. Given the distance between the faults and the stations, we expect, however, the surface displacements to be sensitive to the seismic moment rather than to the fault geometry and slip individually. We verified this by creating a model for aseismic slip in which the same seismic moment as in the model with fixed fault size is accommodated by an increase in both slip and rupture area, such that the ratio between slip and fault length (and hence the stress drop) remains constant. We found that this model gives the same adjusted R^2 value as the model with fixed fault size. Therefore, the factor k should be interpreted more generically as a ratio of moments rather than slip. Assuming constant k for all faults is also a simplification; this value should be considered as an average value relating the total aseismic/seismic slip on all the faults.

5.4. Model 3 — Seismicity + Aseismic Slip + Opening on Dike

The aseismic slip source is also tested in combination with a tensile source with the geometry described in section 5.2 (resulting in a model with 2 degrees of freedom). We also tested the hypothesis that the aseismic slip was released by a pair of normal faults above the dike: we used 12 km long faults with a dip of 60° and vertical extent between 0 and 5 km (i.e., between the surface and the uppermost edge of the dike). We assumed uniform slip with a purely normal mechanism. This model is marked Model 3(B) in Table 2 (using faults with 45° dip results in nearly identical $\bar{R}^2$ values).

6. Results

In order to assess the effect of data uncertainties on the model ranking, we compare the calculated $\bar{R}^2$ values for a set of 10^5 perturbed data realizations. These are obtained from Monte Carlo sampling, assuming data errors to be Gaussian and uncorrelated. We find that models without aseismic slip outperform Model 3 only for 3% of the iterations (Table 2).

The model including only seismic source has the worst performance (Figure 8). The modeled horizontal displacement vectors on Kozushima, Niijima, and Shikinejima have approximately the correct orientation, but their modules are too small; the vertical displacements are also underestimated. The variance reduction of this model is $R^2 = 0.39$, and only 23% of the 3-D baseline displacement between the Kozushima and Niijima stations is explained by coseismic deformation. We deduce that aseismic deformation is taking place during the burst.

The preferred model ($\bar{R}^2 = 0.89$; see Table 2) includes a combination of aseismic slip and opening on a dike (Model 3). Aseismic slip amounts to a geodetic moment of $1.3 \pm 0.4 \times 10^{18}$ N m, while the dike opening corresponds to $7.3 \pm 1.8 \times 10^{17}$ N m (using the definition of seismic moment for a mode-I crack given by

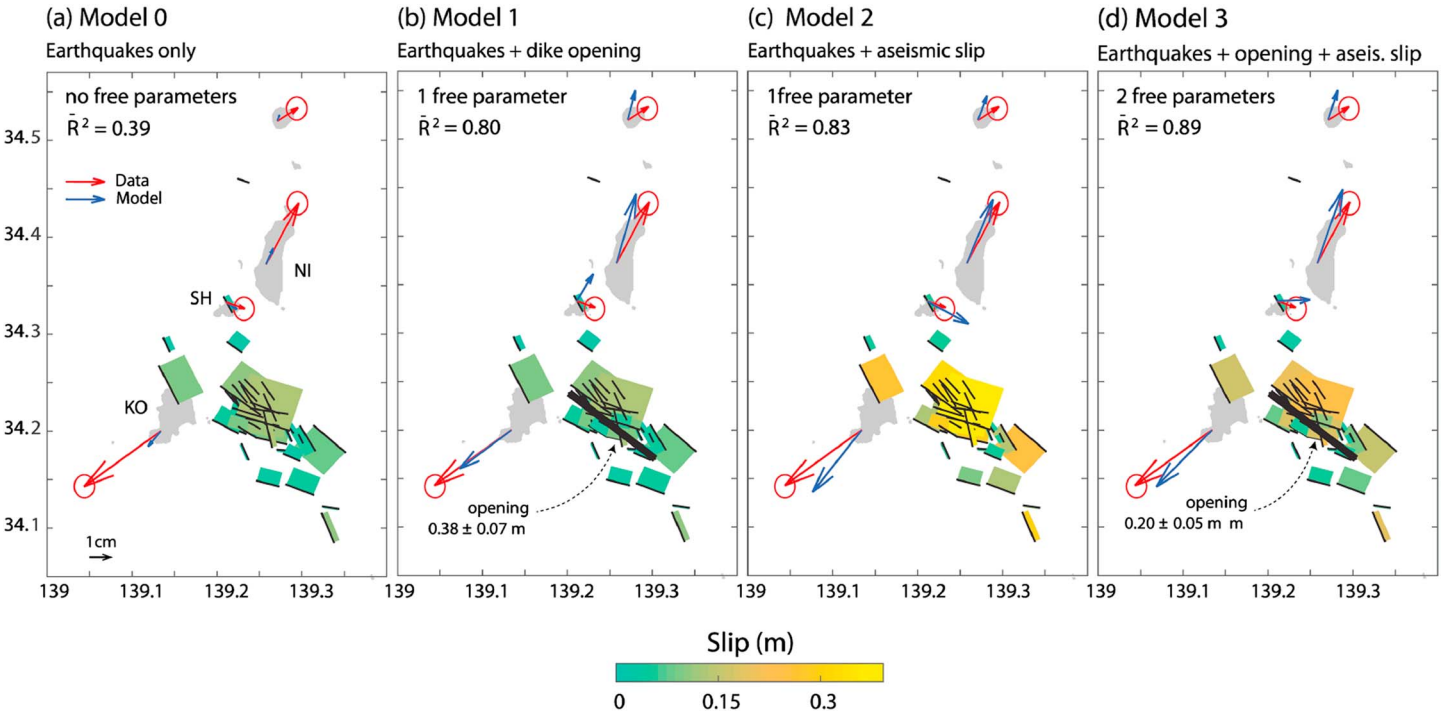

Figure 8. Comparison of observed (red) and modeled (blue) surface deformation estimated from various combinations of seismicity, opening, and aseismic slip. Thin black lines indicate the upper edge of slip models. Red ellipses indicate GPS horizontal error.

Pollard and Segall [1987]). In contrast, earthquakes have a seismic moment of 7.35×10^{17} N m. Based on the ratios of these moments, these results imply that only between 18 and 34% of the observed deformation is caused by dike opening. This corresponds to 1.1 – 2.1 cm, comparable to the daily displacements observed in the 10 days before and after the burst (1.1 ± 0.7 cm) caused by the ongoing dike thickening [*Ito and Yoshioka*, 2002; *Toda et al.*, 2002].

These results indicate that the occurrence of both opening on the dike and additional aseismic slip on the faults is strongly supported by the data, also when considering uncertainties. The tensile source model alone cannot explain the east southeast motion of Shikinejima. This result is robust with respect to dike geometry, since the orientation of the displacement vector on Shikinejima would not substantially change for a different dike length or depth. We note that the deformation recorded in the previous day on this island has the same orientation, suggesting that aseismic slip may have started before the onset of seismicity. This is consistent with other episodes of aseismic slip preceding seismic activity [*Peng and Gomberg*, 2010]. The anomalous orientation of the deformation on Shikinejima was also found by *Hughes* [2010] for the entire duration of the swarm. As indicated by the authors, this suggests that slow slip with a strike-slip component was also taking place at other times during the intrusion.

The other migrating bursts present similarities with the largest one, such as similar focal mechanisms and propagation speeds. However, these events do not present anomalous GPS signals due to their smaller size and larger distance to the GPS stations. We estimate an upper bound to the expected baseline displacement between Kozushima and Niijima by assuming that the other bursts had the same fraction of seismic/aseismic moment as the one on 3 August and scaling the deformation observed on this day by the ratio of seismic moments of each burst and the largest one. In reality, the displacement would be smaller since they are farther away from the stations. We find that for two bursts the expected displacement would be slightly above the reported error and below the measurement error for the others. Therefore, it is plausible that also in those cases aseismic slip took place.

7. Discussion

Based on our results, seismicity alone does not explain the observed deformation: opening of a vertical tensile dislocation and aseismic slip are necessary to a good fit of the data.

As for the tensile source, a plausible hypothesis that we have not yet discussed is that the deformation and the accompanying migration of the burst earthquakes may have been directly caused by additional, smaller-scale magma migration, such as due to the development of finger-shaped magmatic protuberances at the upper edge of the dike, as observed both in laboratory experiments [*Touvet et al.*, 2011] and in the field [*Poland et al.*, 2004]. However, several observations let us discard this hypothesis in favor of a simple background opening of the dike: (1) The background dike opening in the days preceding and following the largest burst is of the same order of magnitude as that in the day during the burst, (2) The burst propagation speed is 4–5 times larger than the propagation velocity of the dike at injection onset, and (3) The opening moment is smaller than the shear moment, suggesting that opening is not driving the migration. Thus, our analysis supports the interpretation that the continuous supply of magma was causing the dike to grow slowly so that the observed tensile deformation came mostly from its thickening, and the bursts were caused indirectly by accumulation of tensile stresses above the dike.

As for the aseismic shear slip accompanying the bursts, the most plausible hypothesis is that ruptures had an aseismic component. This is supported by modeling of the crustal deformation data and also suggested by the migration of the burst hypocenters, analogous to the migration found in other slow slip events accompanied by significant aseismic slip. Moreover, the inferred duration and total moment for the largest burst is comparable to tectonic earthquake swarms associated to slow slip events [*Peng and Gomberg*, 2010; *Gao et al.*, 2012].

Numerical models indicate that the fraction of seismic to aseismic slip can vary depending on asperity size [*Chen and Lapusta*, 2009] and a given fault area can alternate between both types of slip [*Kato*, 2014]. Time-dependent, fluid-related processes such as thermal pressurization and dilatancy also allow for both types of slip on the same fault. Therefore, it is not surprising that mixed modes of moment release take place in nature, spanning a continuum between purely seismic and purely aseismic events [*Peng and Gomberg*, 2010].

As mentioned above, large aseismic slip has been identified for several dikes in the past. In most cases, seismic and aseismic slip were modeled based on a small number (one to two) or normal faults extending along most of the dike [*Nobile et al.*, 2012; *Pallister et al.*, 2010; *Xu et al.*, 2016], although for very long dikes a more complex fault geometry was used [*Wright et al.*, 2006; *Grandin et al.*, 2009]. The good performance of our Model 3(B) shows that a pair of long normal faults may be satisfactory models for the observed crustal deformation, even though the data are best explained by aseismic slip on the same faults as the earthquakes (Model 3). Figure 6 shows that the focal mechanisms are composed of a mixture of normal, strike-slip, and oblique events, with different *P* and *B* axes but uniform tensile axis. Because of the large component of normal faulting in the focal mechanisms, it is expected that Model 3 produces a deformation pattern quite similar to Model 3(B). Indeed, Figure 9 indicates that deformation predicted by the two models is very similar in the NE and SW quadrants (with respect to the position of the source), where the displacement vectors point away from the source. This orientation is expected for both normal and strike-slip focal mechanisms with *T* axis in the NE-SW direction, such as those observed here. From the deformation on Nijima and Kozushima, the two models are therefore difficult to distinguish. On the other hand, more pronounced differences can be seen in the NW and SE quadrants. Dip slip on normal faults produces little deformation in these areas (which are close to the nodal planes of the normal fault plane solutions), while Model 3 predicts displacements pointing toward the sources. This is expected for vertical strike-slip mechanisms with *P* axis in the NW-SE direction, such as many of the events shown in Figure 6. Therefore, the displacement observed in Shikinejima is more consistent with Model 3, leading to the higher $\bar{R}^2$ value. Our preferred interpretation for the aseismic deformation is slow slip on a set of nonaligned faults. Given the overall similarities of the deformation fields, we point out that without additional information, such as focal mechanisms or direct observations of surface faulting, it may generally be difficult to establish whether deformation is localized on few major faults or distributed across a more complex fault system. Finally, we point out that these are only two examples of plausible slip models giving rise to the observed deformation. Alternative models, including, for example, shear on a strike slip at the NW end of the dike, have also been put forward [*Hughes*, 2010; *Maccaferri et al.*, 2015].

We found that during the earthquake burst, the moment released by aseismic shear motion exceeded the moment from opening by a factor of 2. This value is larger than previous estimates for other diking episodes (by about 10–100%; see Figure S1 in the supporting information). Our study focuses on the short timescale of the earthquake burst: the aseismic slip takes place within 24 h (the interval between GPS measurements), and most likely in the ~13 h during which seismicity is high. On the other hand, previous studies based on

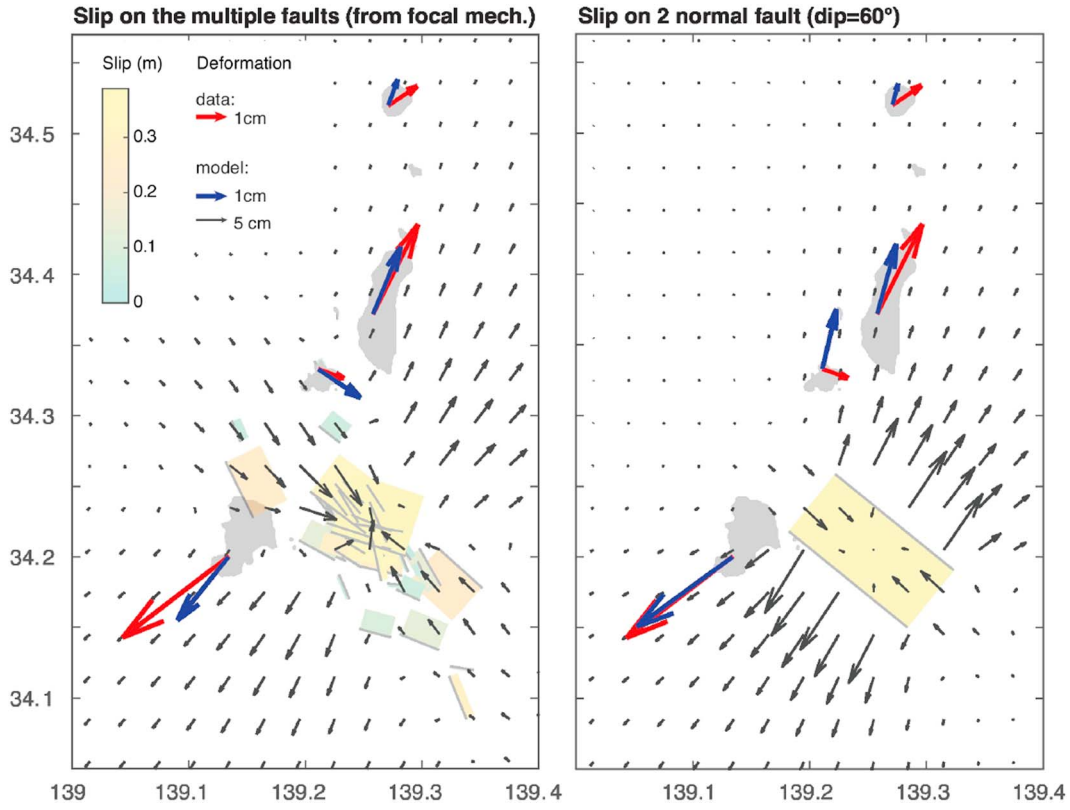

Figure 9. Comparison of surface deformation induced by the aseismic slip component of Model 3 and Model 3(B), showing the different patterns expected from distributed slip versus slip on a set of normal faults. Large arrows are values of surface deformation at the GPS stations, and small arrows indicate the modeled surface deformation pattern (note the different scale).

InSAR evaluated the ratio of shear-to-opening moment over longer time intervals (days to weeks). The difference between these results may therefore indicate that aseismic slip preferentially occurs during intermittent, short-duration events.

One possible explanation for the bursts is fluid flow through a highly fractured rock volume, as suggested for previously observed seismic swarms [*Hainzl et al.*, 2012, 2016; *Shelly et al.*, 2013, 2016]. The existence of fault-fracture meshes, composed of shear faults connecting opening fractures, has been invoked by *Hill* [1977] to explain seismic swarms in extensional settings. *Passarelli et al.* [2015a] demonstrated that these concepts explain the focal mechanisms of the Miyakejima dike intrusion: focal mechanisms indicate a NE-SW σ_3 (consistent with the dike orientation) and a variable σ_1 determined by the stress field of the dike itself (see also Figure 6). Such a fracture mesh controls rock permeability and preferential flow direction: *Sibson* [1996] showed that permeability is enhanced in the σ_2 direction, along which opening and shear fractures connect. For normal faults, this leads to preferential flow along strike; for strike-slip faults, enhanced vertical permeability is expected. In our case, the mesh comprises both faulting styles, so that preferential fluid flow paths may be highly heterogeneous; in general, we note that the direction of swarm migration is consistent with the strike of normal faulting events, which are predominant (Figure 6).

Another feature of seismicity in a fault-fracture mesh is the occurrence of fault valve behavior [*Sibson*, 1990]. Inactive faults normally act as impermeable seals, trapping fluids until pressure reaches a sufficient level for rupture to occur; then, slip on the faults causes a sudden increase in permeability, allowing fluid to flow. The presence of faults with different orientation could enhance this process, since it is more likely that a given fault would cross the preferential flow path established by other faults. This mechanism naturally leads to episodic seismicity, as observed in this study. The spatial relationship between bursts (with sequences often starting where a previous burst arrested) is in agreement with fault valve behavior: a seismic burst may stop when fluid encounters a permeability barrier and remains trapped. This leads to pressure buildup, until the fault slips allowing fluid flow and a new burst.

On the other hand, we note that seismicity migrates much faster than in previously documented cases of fluid-induced seismicity [e.g., *Shelly et al.*, 2013, 2016; *Shapiro and Dinske*, 2009]. Assuming that seismicity is driven by fluid flow, we fit a diffusion curve to the distance-time plot [*Shapiro and Dinske*, 2009]. At time t, the position of the seismicity front (r) driven by pore pressure diffusion is given by

$$r = \sqrt{4\pi D t} \tag{3}$$

where D is the diffusivity. We find that the diffusivity inferred by fitting a diffusion curve to the 3 August burst ($D = 130$ m^2/s) is more than 1 order of magnitude larger than previous values. *Talwani et al.* [2007] collected diffusivity estimates from over 90 instances of natural and induced seismicity and found D to be in the range 0.03–3 m^2/s. They argue that values of permeability outside this range lead to aseismic behavior and in particular that higher diffusivities allow fluid to flow through fractures without inducing seismicity.

An alternative explanation is that seismicity is not directly driven by fluid flow but by an episode of aseismic slip similar to those observed in other tectonic settings and sometimes associated with injected fluids [*Bourouis and Bernard*, 2007; *Wei et al.*, 2015]. In our case, this is supported by the occurrence of aseismic slip inferred geodetically: our inversions, although not unique, indicate that aseismic slip located in the vicinity of the earthquakes is plausible. Moreover, the migration velocity is similar to observed slow slip events. In this interpretation, the relative location of the bursts can be explained by triggering by static stress transfer: each bursts (or faulting episode) creates stresses around its perimeter, where displacement gradients and consequently stresses are largest, determining the most likely location where the next bursts initiate.

The aseismic release may have been facilitated by several factors that have been previously associated with slow ruptures: (1) weak rheology of upper crustal layers [see *Passarelli et al.*, 2015a]; (2) presence of magmatic fluids released during magma degassing increasing pore pressure; (3) low confining stress, also enhanced by tensile stresses from the dike on faults above it (the latter tends to favor slow slip based on a linear stability analysis [*Ruina*, 1983] and by numerical models [*Segall and Bradley*, 2012; *Liu and Rice*, 2007]); and (4) stress heterogeneity (in our case, associated with the variability in fault orientation), which has been suggested to facilitate a combination of aseismic slip and swarms over large seismic ruptures [*Saffer and Wallace*, 2015; *Holtkamp and Brudzinski*, 2014].

8. Conclusions

In this study we document the occurrence of a mixed seismic-aseismic shear slip episode during a dike intrusion. The presence of fluids and low normal stresses on faults above dikes likely make them susceptible to creep and seismic swarms, so that similar intermittent slip episodes may be common and account for a significant fraction of strain release. The bursts have a duration and total (seismic + aseismic) moment comparable to those associated with purely tectonic slow slip events but differ from them for the inhomogeneity of the focal mechanisms. Thus, our analysis points at the existence of "volcanotectonic" seismic swarms indirectly caused by volcanic processes but driven by a slow release of accumulated strain rather than directly by the propagation of magma. Further studies are needed to better constrain the factors leading to seismic or aseismic strain release in these areas and how these events differ from slow slip episodes in other tectonic settings.

Acknowledgments
Data used in this article are from the Japan Meteorological Agency (JMA) and Japan National Research Institute of Earth Science and Disaster Prevention (NIED). Any request of data should be addressed directly to those institutions. We thank Simone Cesca for providing the focal mechanisms clustering code. This research was funded by the European Union, ERC StG "CCMP-POMPEI", 240583 and Supersite project MED-SUV, grant N. 308665. C.C. was additionally supported by a Career Support fellowship provided by the graduate school GeoSim.

References

Ágústsdóttir, T., J. Woods, T. Greenfield, R. G. Green, R. S. White, T. Winder, B. Brandsdóttir, S. Steinthórsson, and H. Soosalu (2016), Strike-slip faulting during the 2014 Bárðarbunga-Holuhraun dike intrusion, central Iceland, *Geophys. Res. Lett.*, *43*(4), 1495–1503, doi:10.1002/2015GL067423.

Baer, G., Y. Hamiel, G. Shamir, and R. Nof (2008), Evolution of a magma-driven earthquake swarm and triggering of the nearby Oldoinyo Lengai eruption, as resolved by InSAR, ground observations and elastic modeling, East African Rift, 2007, *Earth Planet. Sci. Lett.*, *272*(1–2), 339–352, doi:10.1016/j.epsl.2008.04.052.

Belachew, M., C. Ebinger, D. Cote, D. Keir, J. V. Rowland, J. O. S. Hammond, and A. Ayele (2011), Comparison of dike intrusions in an incipient seafloor-spreading segment in Afar, Ethiopia: Seismicity perspectives, *J. Geophys. Res.*, *116*, B06405, doi:10.1029/2010JB007908.

Belachew, M., C. Ebinger, and D. Coté (2013), Source mechanisms of dike-induced earthquakes in the Dabbahu-Manda Hararo rift segment in Afar, Ethiopia: Implications for faulting above dikes, *Geophys. J. Int.*, *192*(3), 907–917, doi:10.1093/gji/ggs076.

Beroza, G. C., and S. Ide (2011), Slow earthquakes and nonvolcanic tremor, *Annu. Rev. Earth Planet. Sci.*, *39*(1), 271–296, doi:10.1146/annurev-earth-040809-152531.

Borghi, A., A. Aoudia, F. Javed, and R. Barzaghi (2016), Precursory slow-slip loaded the 2009 L'Aquila earthquake sequence, *Geophys. J. Int.*, *205*(2), 776–784, doi:10.1093/gji/ggw046.

Bourouis, S., and P. Bernard (2007), Evidence for coupled seismic and aseismic fault slip during water injection in the geothermal site of Soultz (France), and implications for seismogenic transients, *Geophys. J. Int.*, *169*(2), 723–732, doi:10.1111/j.1365-246X.2006.03325.x.

Brandsdóttir, B., and P. Einarsson (1979), Seismic activity associated with the September 1977 deflation of the Krafla central volcano in northeastern Iceland, *J. Volcanol. Geotherm. Res.*, *6*(3–4), 197–212, doi:10.1016/0377-0273(79)90001-5.

Brodsky, E. E., and J. Mori (2007), Creep events slip less than ordinary earthquakes, *Geophys. Res. Lett.*, *34*, L16309, doi:10.1029/2007GL030917.

Buck, W. R., L. L. Lavier, and A. N. B. Poliakov (2005), Modes of faulting at mid-ocean ridges, *Nature*, *434*(7034), 719–723, doi:10.1038/nature03358.

Calais, E., et al. (2008), Strain accommodation by slow slip and dyking in a youthful continental rift, East Africa, *Nature*, *456*(7223), 783–787, doi:10.1038/nature07478.

Cesca, S., A. T. Ízen, and T. Dahm (2014), Seismicity monitoring by cluster analysis of moment tensors, *Geophys. J. Int.*, *196*(3), 1813–1826, doi:10.1093/gji/ggt492.

Chen, T., and N. Lapusta (2009), Scaling of small repeating earthquakes explained by interaction of seismic and aseismic slip in a rate and state fault model, *J. Geophys. Res.*, *114*, B01311, doi:10.1029/2008JB005749.

Gao, H., D. A. Schmidt, and R. J. Weldon II (2012), Scaling relationships of source parameters for slow slip events, *Bull. Seismol. Soc. Am.*, *102*(1), 352–360, doi:10.1785/0120110096.

Geshi, N., V. Acocella, and J. Ruch (2012), From structure- to erosion-controlled subsiding calderas: Evidence thresholds and mechanics, *Bull. Volcanol.*, *74*(6), 1553–1567, doi:10.1007/s00445-012-0617-x.

Grandin, R., et al. (2009), September 2005 Manda Hararo-Dabbahu rifting event, Afar (Ethiopia): Constraints provided by geodetic data, *J. Geophys. Res.*, *114*, B08404, doi:10.1029/2008JB005843.

Habermann, R. E. (1983), Teleseismic detection in the Aleutian Island Arc, *J. Geophys. Res.*, *88*(3), 5056–5064.

Hainzl, S., T. Fischer, and T. Dahm (2012), Seismicity-based estimation of the driving fluid pressure in the case of swarm activity in Western Bohemia, *Geophys. J. Int.*, *191*, 271–281, doi:10.1111/j.1365-246X.2012.05610.x.

Hainzl, S., T. Fischer, H. Čermàkova, M. Bachura, and J. Vlček (2016), Aftershocks triggered by fluid intrusion: Evidence for the aftershock sequence occurred 2014 in West Bohemia/Vogtland, *J. Geophys. Res. Solid Earth*, *121*, 2575–2590, doi:10.1002/2015JB012582.

Hill, D. P. (1977), A model for earthquake swarms, *J. Geophys. Res.*, *82*, 1347–1352.

Holtkamp, S., and M. R. Brudzinski (2014), Megathrust earthquake swarms indicate frictional changes which delimit large earthquake ruptures, *Earth Planet. Sci. Lett.*, *390*, 234–243, doi:10.1016/j.epsl.2013.10.033.

Hughes, G. R. (2010), Investigations of magmatic end-members: Silicic magma chambers and mafic dikes, PhD thesis, Stanford Univ., Stanford, Calif.

Ide, S., G. C. Beroza, D. R. Shelly, and T. Uchide (2007), A scaling law for slow earthquakes, *Nature*, *447*(7140), 76–79, doi:10.1038/nature05780.

Ito, T., and S. Yoshioka (2002), A dike intrusion model in and around Miyakejima, Niijima and Kozushima in 2000, *Tectonophysics*, *359*(1–2), 171–187, doi:10.1016/S0040-1951(02)00510-3.

Kato, A., K. Obara, T. Igarashi, H. Tsuruoka, S. Nakagawa, and N. Hirata (2012), Propagation of slow slip leading up to the 2011 M_w9.0 Tohoku-oki earthquake, *Science*, *335*, 705–709, doi:10.1126/science.1215141.

Kato, N. (2014), Deterministic chaos in a simulated sequence of slip events on a single isolated asperity, *Geophys. J. Int.*, *198*(2), 727–736, doi:10.1093/gji/ggu157.

Kumagai, H., T. Ohminato, M. Nakano, M. Ooi, A. Kubo, H. Inoue, and J. Oikawa (2001), Very-long-period seismic signals and caldera formation at Miyake Island, Japan, *Science*, *293*(5530), 687–690, doi:10.1126/science.1062136.

Linde, A. T., M. T. Gladwin, M. J. S. Johnston, R. L. Gwyther, and R. G. Bilham (1996), A slow earthquake sequence on the San Andreas fault, *Nature*, *383*(6595), 65–68, doi:10.1038/383065a0.

Liu, Y., and J. R. Rice (2007), Spontaneous and triggered aseismic deformation transients in a subduction fault model, *J. Geophys. Res.*, *112*, B09404, doi:10.1029/2007JB004930.

Lohman, R. B., and J. J. McGuire (2007), Earthquake swarms driven by aseismic creep in the Salton Trough, California, *J. Geophys. Res.*, *112*, B04405, doi:10.1029/2006JB004596.

Maccaferri, F., E. Rivalta, L. Passarelli, and Y. Aoki (2015), On the mechanisms governing dike arrest: Insight from the 2000 Miyakejima dike injection, *Earth Planet. Sci. Lett.*, *434*, 64–74, doi:10.1016/j.epsl.2015.11.024.

Marsan, D. (2003), Triggering of seismicity at short timescales following Californian earthquakes, *J. Geophys. Res.*, *108*(B5), 1–14, doi:10.1029/2002JB001946.

Mastin, L. G., and D. D. Pollard (1988), Surface deformation and shallow dike intrusion processes at Inyo Craters, Long Valley, California, *J. Geophys. Res.*, *93*(B11), 13,221–13,235, doi:10.1029/JB093iB11p13221.

Matthews, M. V., and P. A. Reasenberg (1988), Statistical methods for investigating quiescence and other temporal seismicity patterns, *Pure Appl. Geophys.*, *126*(2–4), 357–372, doi:10.1007/BF00879003.

Maury, J., S. Ide, V. M. Cruz-Atienza, V. Kostoglodov, G. González-Molina, and X. Pérez-Campos (2016), Comparative study of tectonic tremor locations: Characterization of slow earthquakes in Guerrero, Mexico, *J. Geophys. Res. Solid Earth*, *121*, 5136–5151, doi:10.1002/2016JB013027.

Minson, S. E., D. S. Dreger, R. Bürgmann, H. Kanamori, and K. M. Larson (2007), Seismically and geodetically determined nondouble-couple source mechanisms from the 2000 Miyakejima volcanic earthquake swarm, *J. Geophys. Res.*, *112*, B10308, doi:10.1029/2006JB004847.

Nobile, A., C. Pagli, D. Keir, T. J. Wright, A. Ayele, J. Ruch, and V. Acocella (2012), Dike-fault interaction during the 2004 Dallol intrusion at the northern edge of the Erta Ale Ridge (Afar, Ethiopia), *Geophys. Res. Lett.*, *39*, L19305, doi:10.1029/2012GL053152.

Pallister, J. S., et al. (2010), Broad accommodation of rift-related extension recorded by dyke intrusion in Saudi Arabia, *Nat. Geosci.*, *3*(10), 705–712, doi:10.1038/ngeo966.

Passarelli, L., E. Rivalta, S. Cesca, and Y. Aoki (2015a), Stress changes, focal mechanisms, and earthquake scaling laws for the 2000 dike at Miyakejima (Japan), *J. Geophys. Res. Solid Earth*, *120*, 4130–4145, doi:10.1002/2014JB011504.

Passarelli, L., S. Hainzl, S. Cesca, F. Maccaferri, M. Mucciarelli, D. Roessler, F. Corbi, T. Dahm, and E. Rivalta (2015b), Aseismic transient driving the swarm-like seismic sequence in the Pollino range, Southern Italy, *Geophys. J. Int.*, *201*, 1553–1567, doi:10.1093/gji/ggv111.

Pedersen, R., F. Sigmundsson, and P. Einarsson (2007), Controlling factors on earthquake swarms associated with magmatic intrusions; Constraints from Iceland, *J. Volcanol. Geotherm. Res.*, *162*(1), 73–80, doi:10.1016/j.jvolgeores.2006.12.010.

Peng, Z., and J. Gomberg (2010), An integrated perspective of the continuum between earthquakes and slow-slip phenomena, *Nat. Geosci.*, *3*(9), 599–607, doi:10.1038/ngeo940.

Poland, M. P., J. H. Fink, and L. Tauxe (2004), Patterns of magma flow in segmented silicic dikes at Summer Coon volcano, Colorado: AMS and thin section analysis, *Earth Planet. Sci. Lett.*, *219*(1–2), 155–169, doi:10.1016/S0012-821X(03)00706-4.

Pollard, D. D., and P. Segall (1987), Theoretical displacements and stresses near fractures in rock: With applications to faults, joints, veins, dikes, and solution surfaces, in *Fracture Mechanics of Rock*, vol. 277, pp. 277–349, Academic Press, London, doi:10.1016/B978-0-12-066266-1.50013-2.

Reasenberg, P. A., and R. W. Simpson (1992), Response of regional seismicity to the static stress change produced by the Loma Prieta earthquake, *Science*, *255*(5052), 1687–1690.

Rivalta, E. (2010), Evidence that coupling to magma chambers controls the volume history and velocity of laterally propagating intrusions, *J. Geophys. Res.*, *115*, B07203, doi:10.1029/2009JB006922.

Rowland, J. V., E. Baker, C. J. Ebinger, D. Keir, T. Kidane, J. Biggs, N. Hayward, and T. J. Wright (2007), Fault growth at a nascent slow-spreading ridge: 2005 Dabbahu rifting episode, Afar, *Geophys. J. Int.*, *171*(3), 1226–1246, doi:10.1111/j.1365-246X.2007.03584.x.

Rubin, A. M. (1992), Dike-induced faulting and graben subsidence in volcanic rift zones, *J. Geophys. Res.*, *97*(91), 1839–1858, doi:10.1029/91JB02170.

Ruch, J., T. Wang, W. Xu, and S. Jónsson (2016), Oblique rift opening revealed by reoccurring magma injection in central Iceland, *Nat. Commun.*, *7*, 12352, doi:10.1038/ncomms12352.

Ruina, A. (1983), Slip instability and state variable friction law, *J. Geophys. Res.*, *88*, 10,359–10,370, doi:10.1029/JB088iB12p10359.

Saffer, D. M., and L. M. Wallace (2015), The frictional, hydrologic, metamorphic and thermal habitat of shallow slow earthquakes, *Nature Geosci.*, *8*(8), 594–600, doi:10.1038/ngeo2490.

Sakai, S., et al. (2001), Magma migration from the point of view of seismic activity in the volcanism of Miyake-jima Island in 2000, *J. Geogr.*, *110*(2), 145–155.

Segall, P., and A. M. Bradley (2012), The role of thermal pressurization and dilatancy in controlling the rate of fault slip, *J. Appl. Mech.*, *79*(3), 31,013, doi:10.1115/1.4005896.

Segall, P., and D. D. Pollard (1980), Mechanics of discontinuous faults, *J. Geophys. Res.*, *85*(B8), 4337–4350, doi:10.1029/JB085iB08p04337.

Segall, P., E. K. Desmarais, D. Shelly, A. Miklius, and P. Cervelli (2006), Earthquakes triggered by silent slip events on Kīlauea volcano, Hawaii, *Nature*, *442*, 71–74, doi:10.1038/nature04938.

Shapiro, S. A., and C. Dinske (2009), Fluid-induced seismicity: Pressure diffusion and hydraulic fracturing, *Geophys. Prospect.*, *57*, 301–310, doi:10.1111/j.1365-2478.2008.00770.x.

Shelly, D. R., S. C. Moran, and W. A. Thelen (2013), Evidence for fluid-triggered slip in the 2009 Mount Rainier, Washington earthquake swarm, *Geophys. Res. Let.*, *40*, 1506–1512, doi:10.1002/grl.50354.

Shelly, D. R., W. L. Ellsworth, and D. P. Hill (2016), Fluid-faulting evolution in high definition: Connecting fault structure and frequency-magnitude variations during the 2014 Long Valley Caldera, California, earthquake swarm, *J. Geophys. Res. Solid Earth*, *121*, 1776–1795, doi:10.1002/2015JB012719.

Shuler, A., and M. Nettles (2012), Earthquake source parameters for the 2010 western Gulf of Aden rifting episode, *Geophys. J. Int.*, *190*(2), 1111–1122, doi:10.1111/j.1365-246X.2012.05529.x.

Sibson, H. (1990), Conditions for fault-valve behaviour, *Deformation Mech. Rheol. Tectonic, Knipe R. J*, *54*, 15–28.

Sibson, H. (1996), Structural permeability of fluid-driven fault-fracture, *J. Struct. Geol.*, *18*(8), 1031–1042.

Solomon, S., P. Huang, and L. Meinke (1988), The seismic moment budget of slowly spreading ridges, *Nature*, *334*, 58–60, doi:10.1038/334058a0.

Talwani, P., L. Chen, and K. Gahalaut (2007), Seismogenic permeability, k_s, *J. Geophys. Res.*, *112*, B07309, doi:10.1029/2006JB004665.

Toda, S., R. S. Stein, and T. Sagiya (2002), Evidence from the AD 2000 Izu Islands earthquake swarm that stressing rate governs seismicity, *Nature*, *419*(6902), 58–61, doi:10.1038/nature00997.

Touvet, T., N. J. Balmforth, R. V. Craster, and B. R. Sutherland (2011), Fingering instability in buoyancy-driven fluid-filled cracks, *J. Fluid Mech.*, *672*, 60–77, doi:10.1017/S0022112010005860.

Ukawa, M., and H. Tsukahara (1996), Earthquake swarms and dike intrusions off the east coast of Izu Peninsula, central Japan, *Tectonophysics*, *253*(3), 285–303, doi:10.1016/0040-1951(95)00077-1.

Villegas-Lanza, J. C., J.-M. Nocquet, F. Rolandone, M. Vallée, H. Tavera, F. Bondoux, T. Tran, X. Martin, and M. Chlieh (2015), A mixed seismic-aseismic stress release episode in the Andean subduction zone, *Nat. Geosci.*, *9*(2), 150–154, doi:10.1038/ngeo2620.

Wei, M., Y. Kaneko, Y. Liu, and J. J. McGuire (2013), Episodic fault creep events in California controlled by shallow frictional heterogeneity, *Nat. Geosci.*, *6*(7), 566–570, doi:10.1038/ngeo1835.

Wei, M., Y. Liu, Y. Kaneko, J. J. McGuire, and R. Bilham (2015), Dynamic triggering of creep events in the Salton Trough, Southern California by regional $M>5.4$ earthquakes constrained by geodetic observations and numerical simulations, *Earth Planet. Sci. Lett.*, *427*, 1–10, doi:10.1016/j.epsl.2015.06.044.

Wells, D., and K. Coppersmith (1994), Updated empirical relationships among magnitude, rupture length, rupture area, and surface displacement, *Bull. Seismol. Soc. Am.*, *84*(4), 974–1002.

Wiemer, S. (2001), A software package to analyze seismicity: ZMAP, *Seismol. Res. Lett.*, *72*, 373–382.

Wright, T. J., C. Ebinger, J. Biggs, A. Ayele, G. Yirgu, D. Keir, and A. Stork (2006), Magma-maintained rift segmentation at continental rupture in the 2005 Afar dyking episode, *Nature*, *442*(7100), 291–294, doi:10.1038/nature04978.

Xu, W., S. Jonsson, F. Corbi, and E. Rivalta (2016), Graben formation and dike arrest during the 2009 Harrat Lunayyir dike intrusion in Saudi Arabia: Insights from InSAR, stress calculations and analog experiments, *J. Geophys. Res. Solid Earth*, *121*, 1–23, doi:10.1002/2015JB012505.

Yamaoka, K., M. Kawamura, F. Kimata, N. Fujii, and T. Kudo (2005), Dike intrusion associated with the 2000 eruption of Miyakejima Volcano, Japan, *Bull. Volcanol.*, *67*(3), 231–242, doi:10.1007/s00445-004-0406-2.